Coherent contribution of consecutive electron rescatterings in the extreme ultraviolet supercontinuum

M. Dashcasan* and E. Barati
Pulsed Laser Research Group, Center of Laser Science and Technology, P. O. Box 14657-33441, Tehran
(Received 29 January 2014; published 15 April 2014)

In this article, coherent contributions of high-order quantum paths are proposed to generate a highly efficient and fine appearance attosecond pulse. We show how the electron dynamics of the high-order harmonics evolves so that harmonics are generated by a helium atom exposed to the two-color waveform composed of sub-one-cycle pulses. The leading and the trailing of the pulse is constructed by the near-infrared driving pulse and a midinfrared control pulse, respectively, thereby tunnel ionization and recombination are effectively manipulated. This waveform not only broadens the bandwidth but also leads to the contribution of high-order rescatterings in the generated supercontinuum and thereby enhances the harmonic yields. Whereas the effective duration of the waveform is lesser than the midinfrared pulse, with prolonging the pulse trailing, the long path of first-order rescattering is completely suppressed and high-order rescatterings of different electron trajectories appear. The most interesting feature is that under optimized conditions, the short paths of consecutive rescatterings coherently contribute in the high-order-harmonic generation process that leads to a fine appearance in the attosecond pulses.

DOI: 10.1103/PhysRevA.89.043412 PACS number(s): 33.80.Wz, 42.65.Ky, 42.65.Re, 32.80.Wr

I. INTRODUCTION

High-order-harmonic generation (HHG) in atoms is a promising scheme to produce trains or isolated attosecond (as) pulses (IAP) in the extreme ultraviolet (XUV) emission and is an attractive test bed for ultrafast coherent control of electron dynamics [1–4]. HHG from a few-cycle driving pulse and the temporal confinement of HHG using polarization gating are the two techniques currently available for creating IAP [5–8]. Recently, Zhao *et al*. produced a 67 as pulse via the latter method, with a 7 fs, 750 nm laser pulse, which is the shortest attosecond pulse known to us [9]. Control of the quantum path of the returning electron via waveform (the combined multi-color fields) is an efficient way to produce a supercontinuum HHG spectrum and IAP. The origin of the high-order-harmonic emission in the XUV range corresponds physically to trajectories that an electron can follow during the generation process. Over one given trajectory the electron motion is described by a three-step model [10,11]: emission into the continuum by tunnel ionization, acceleration by the linearly polarized laser field driving the electron back to the core inducing a recombination, and the emission of a harmonic photon. Among all the possible trajectories, the two first quantum paths, referred to as the "short" and the "long" trajectories, provide the dominant contribution to high-order-harmonic emission in the plateau region; however, their phases are not locked. These contributions evolve and merge to a single path dominating the cutoff region. Interference between quantum paths is detrimental to producing an isolated attosecond pulse, thus, picking out a single quantum path is necessary. At present, various ways of controlling quantum paths are proposed in the multicolor field scheme [12–25].

To obtain high photon energies, the ponderomotive energy of the electron in the laser field given by $Up(\mathrm{eV}) = 9.38 \times 10^{-14} I\ (\mathrm{W/cm^2})\ [\lambda_0(\mu\mathrm{m})]^2$ should be maximized. Based on this equation, in the HHG process, electrons can efficiently tunnel ionized by the intense interaction of an intense near-infrared pulse and atomic gas, and then achieve considerable kinetic energy after traveling freely in the oscillating field. An extremely high driving field will lead to the ionization saturation of the target atom and limit the harmonic yields. On the other hand, a high ionization rate also leads to plasma defocusing of the driving pulse and dephasing of the atomic dipole oscillators, then further decreases the conversion efficiency. Most of the electrons, however, cannot be driven back to parent ions to contribute in high-order-harmonic generation. A midinfrared pulse can improve the HHG cutoff energy but the enhanced electron wave-packet spreading leads to a reduction in harmonic yield [26,27]. Our idea is triggered by what was argued about the ionization and recombination aspects of near-IR and mid-IR pulses, respectively. A synthesized two-color field contains an intense subcycle near-IR laser pulse as the leading part of the waveform for efficient ionization and a subcycle mid-IR pulse as the trailing part of the waveform for efficient recombination. It is clear that prolonging of the leading part of the waveform cannot be done through a mid-IR pulse, because the enhanced electron wave-packet spreading leads to a reduction of the ionization rate. In our previous work [18], we tried to prolong the leading part through the chirped pulse technology and terahertz field. We showed that in spite of the extension of supercontinuum, the harmonics yields intensively drop due to insufficient recombination time. In comparison with the prolonged leading waveform, the waveform presented in this work can produce an XUV supercontinuum that has three main aspects. First, the short path of consecutive rescatterings can coherently contribute in the harmonics spectra in which this also leads to the enhancement of harmonics yields. Second, the harmonic spectrum can be extended up to higher orders. Third, the contribution of the control pulse in the ionization process is reduced, which leads to the reduction of the ionization-induced mismatching of the harmonics in the ionized media at the macroscopic level. It is evident that the contribution of consecutive rescatterings compensates the effects of reduction of accessible electrons on the harmonics yields. In other words, the employment of

*dashcasan@gmail.com

consecutive rescatterings and the reduction of the ionization rate to a reasonable value enhances the harmonic yields and reduces the induced-ionization effects. The first result is the core of this work. High-order rescatterings of the different electron trajectories are not observed using near-IR driving laser wavelengths around 800 nm, and are only present when mid-IR driving fields are used. In our simulations, through a two-color prolonged trailing scheme, they appear during the interaction, and mainly influence the HHG spectra. Here, we attempt to study the electron dynamics by enhancing the wavelength of the control pulse; i.e., we focus on the electron dynamics in a prolonged pulse to see how the trailing of pulse affects the electron dynamics during the harmonic generation process. We show that by exposing atoms to the prolonged trailing pulse containing two-color sub-one-cycle laser fields, high-order rescatterings appear and coherently contribute in the HHG process.

This paper is outlined as follows. In Sec. II, we briefly describe the background physics of the HHG process and the employed numerical method to simulate a pulse-atom interaction. In Sec. III, we discuss how the HHG process in the presence of a prolonged synthesized two-color laser is affected by the control wave. In fact, we gradually lengthen the trailing of pulse to study the quantum paths of different trajectories of returned electrons. Finally, we summarize our important results in the Conclusion section.

II. PHYSICAL MODEL

This section provides a background to theoretical physics and simulation of pulse-atom interactions. The dynamics of an atomic electron in a strong laser field is mainly along the direction of the field. Hence, it is reasonable to model the HHG in 1D by solving the time-dependent Schrödinger equation (TDSE) in the single active electron and dipole approximation. The soft-core potential of a helium atom can be expressed as $V_{\text{atom}}(x) = -1/\sqrt{(b + x^2)}$, where $b = 0.484$ is the softening parameter which corresponds to the ionization potential (I_p) of 24.6 eV for the ground state. The potential due to the combined laser electric field linearly polarized along the x axis can be expressed as

$$V_{\text{laser}}(x,t) = -\vec{E}\cdot\vec{r} = \{E_0 f_0(t+t_d)\cos[\omega_0(t+t_d)] + E_1 f_1(t-t_d)\cos[\omega_1(t-t_d)+\varphi_{\text{CEP}}]\}x. \quad (1)$$

Here t_d is the time delay between the driving and control pulses. E_i and ω_i ($i = 0,1$) are the peak amplitudes and frequencies of the fundamental and control pulses, respectively. $f_i(t) = \exp[-2\ln(t^2/\tau_i^2)]$ presents the profile of both laser fields with corresponding pulse duration τ. φ_{CEP} is the carrier-envelope phase of the control pulse. The one-dimensional time-dependent Schrödinger equation

$$i\frac{\partial\psi(x,t)}{\partial t} = H(t)\psi(x,t) = \left[-\frac{1}{2}\frac{\partial^2}{\partial x^2} + V_{\text{atom}}(x) + V_{\text{laser}}(x,t)\right]\psi(x,t) \quad (2)$$

can be solved numerically by using the Crank-Nicholson scheme and the LAPACK subroutine ZGTSV (complex tridiagonal matrix solver). The initial state in TDSE is the ground state of the system before we turn on the laser ($t = -\infty$). Once the time evolution of the wave function is determined, the time-dependent induced dipole acceleration can be given by means of Ehrenfest's theorem:

$$a(t) = \frac{d^2}{dt^2}\langle x\rangle = -\langle\psi(x,t)|\frac{\partial V}{\partial x} - E(t)|\psi(x,t)\rangle. \quad (3)$$

The harmonic spectrum can be obtained, which is proportional to the modulus squared of the Fourier transform of $a(t)$. By superposing several orders of the harmonics, an ultrashort pulse can be obtained. To analyze the harmonic energy at the photon burst time, we will perform the quantum wavelet analysis via the Gabor transform [28].

In the classical picture, to find the recollision time, we should solve the Newton's equation knowing such time satisfies the equation $x_e(t_r) = 0$, i.e., the electron comebacks to the initial position. It is found that two couple times (t_r, t_i) satisfy the following equation:

$$\int_{t_i}^{t_r} A(t)dt = (t_r - t_i)\,A(t_i). \quad (4)$$

Then the harmonic energy E_h can be obtained through $E_h = 0.5[A(t_r) - A(t_i)]^2 + I_p$; here $A(t)$ is called the electric potential, and t_i and t_r are the ionization and the recombination times, respectively.

III. RESULTS AND DISCUSSION

In order to clearly demonstrate a physical picture of the quantum control in the combined field, we first investigate the HHG process by the electron dynamics in a classical three-step model. In our first attempt, the two-color laser pulse is synthesized by a half-cycle (FWHM) 800-nm driving pulse and a half-cycle 2000-nm control pulse. The time delay between the driving and control pulse is 1.3 fs (half cycle of the driving pulse) and φ_{CEP} is set to be $-\pi$. The intensities of the driving pulse and the control pulse are 2×10^{14} and 1×10^{14} W/cm^2, respectively. Afterwards, to form the synthesized field the wavelength of the control pulse only changes. Note that the intensity of the laser pulse is far below the saturation intensity of the target atom. Then the harmonic efficiency is mainly determined by the ionization rate, according to the three-step model. In this case, the HHG process can be well depicted in terms of classical electron trajectories and the ionization rate. All electron dynamics in the classical picture can be obtained from Figs. 1(a) and 1(b). Figure 1(a) presents the combination of the subcycle 800-nm and 2000-nm laser pulses. Here, the major local maximums of peaks are marked by B, C, and D. We can see that the effective wavelength is increased for this combined pulse, and the intensity of the peaks is also. In Fig. 1(a) it can be seen that owing to the ultrashort duration, the tunneling electron wave packet will be dominantly launched when the laser field reaches a local maximum; i.e., mainly at the peak C where the intensity of the waveform is more intense than peaks B and D. Based on three-step process marked ABC (ionization-acceleration-recombination), ionized electrons in the AB branch are reversed back at peak B and then contribute to harmonics emission up to only the 38th harmonic because of lower ionization efficiency. In the second HHG process BCD, more electrons can be efficiently ionized around peak C. Therefore, the quasifree electrons can obtain

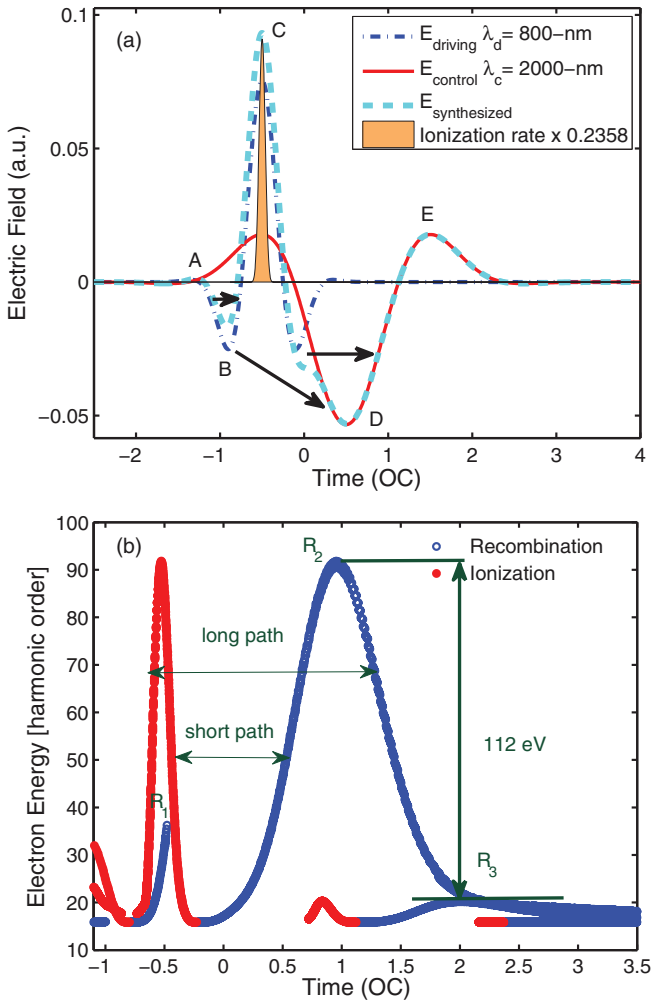

FIG. 1. (Color online) (a) Amplitude of electric fields (vs atomic unit) of the half-cycle 800-nm driving pulse, the half-cycle 2000-nm control pulse, two-color field synthesized by half-cycle 800-nm driving and half-cycle 2000-nm control pulses as a function of time (optical cycle), and the ionization rate in the two-color pulse. (b) Classical sketch of the electron dynamics—ionization and recombination times—in the two-color pulse. The intensities of the driving pulse and the control pulse are 2×10^{14} and 1×10^{14} W/cm^2, respectively. The arrows plot the possible HHG process based on the well-known three-step model.

a higher cutoff energy when the electrons are ionized from the major local ionization peak C and return to emit the HHG radiation at the major local emission peak D. During process CDE, most electrons ionized in CD, because of an insufficient intense field, cannot recomeback to the ion parent in the DE branch of the CDE process, so such electrons can only contribute to harmonics emission up to the 20th harmonic. In the BCD process, the electron spends more time in the acceleration step and also in the return to the parent ion, which is responsible for the extension of the cutoff energy up to the 90th harmonic. Superimposing the longer wavelength field affects the waveform and remarkably increases the amplitude of C, so the ionized electrons gain much more energy from the laser field through the acceleration step. On the other hand, the superimposed field extends the returning step, so it helps to extend the cutoff. Figure 1(b) shows the electron trajectories. The ionization and recombination times are shown by red filled circles and blue open circles, respectively. As shown in this figure, there are three main emission peaks (marked R_1, R_2, and R_3) with maximum harmonic orders 38, 90, and 20, respectively. One can clearly see that the returning probability of the electron path R_1 is much lower than those of R_2 and R_3 owing to the lower ionization rate; thus the harmonic yield for R_1 is much lower than the others. Taking into account the above results, we can conclude that a supercontinuum between the maximum energies of R_2 and R_3 (with the 112 eV) can be generated. Figure 1(b) shows the two quantum paths, namely, the long quantum path (earlier ionization, later recollision) and the short quantum path (later ionization, earlier recollision). It is well known that each emitted harmonic receives these two quantum path contributions and the less modulated supercontinuum contributed by the single quantum path is more beneficial to generate the isolated attosecond pulse. Since Fig. 1(b) shows the two contributing paths in the HHG process, we expect the interference between two paths will take place.

To confirm the above classical prediction, we calculate the harmonic spectrum using TDSE as shown in Fig. 2. For comparison, the harmonic spectrum in the monocycle 800-nm, 3×10^{14} W/cm^2 driving pulse alone is also shown. Note that the monocycle pulse and waveform both have the same intensities. As shown in this figure, the harmonics from 20 to the cutoff becomes continuous. Additionally, the modulation in the supercontinuum, which is due to interferences between short and long quantum paths, regularly happens as was predicted by Fig. 1(b). In comparison to the harmonic spectrum of the 800-nm pulse, the advantages of superimposed subcycle 2000 nm is more characterized. First, the harmonic yields of the generated supercontinuum are several times higher than that of the harmonics at the same orders in the 800-nm

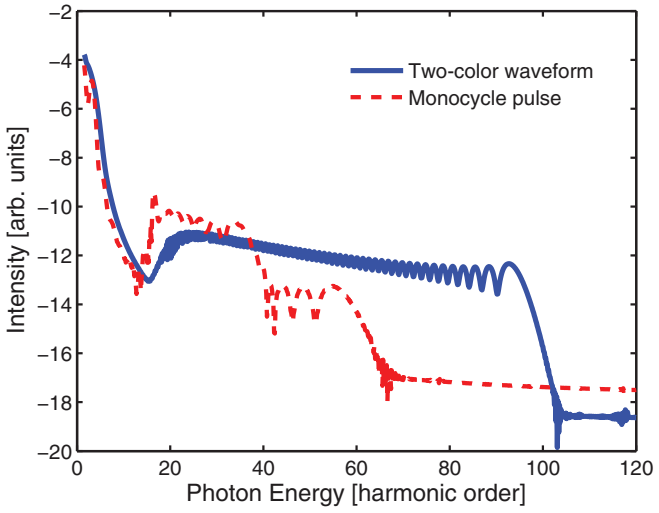

FIG. 2. (Color online) The harmonic spectrum of a helium atom exposed to the two-color field synthesized by half-cycle 800-nm driving and half-cycle 2000-nm control pulses and the monocycle 800-nm driving pulse alone. The intensities of the driving pulse and the control pulse are 2×10^{14} and 1×10^{14} W/cm^2, respectively. The intensity of the monocycle 800-nm driving pulse is 3×10^{14} W/cm^2.

driving pulse alone. Note that in the high-order-harmonic generation process, the second plateau which contains high harmonics is considered. Second, the superimposed subcycle 2000 nm efficiently expands the cutoff up to several tens of order higher than that of the 800-nm pulse. To understand the reasons for such effects, we investigate Fig. 1(a) again. It is seen that the 2000-nm pulse mainly strengthens peak C and affects the ionization process so the harmonics yields can be increased. On the other hand, the superimposed 2000 nm prolongs the trailing of waveform and causes more electrons to have sufficient time to come back to the ion parent. It can be seen that the interference in the plateau middle is much less than its end. Because the harmonics yields in the middle are higher than the end, it therefore helps to obtain an intense attosecond pulse. To address more physical insights and analyze quantum path contributions, we present the time-frequency distributions of HHG through the quantum wavelet transformation of the dipole acceleration $a(t)$. The quantum wavelet transform method not only indicates the emission channels, but also provides the relative intensities between channels, whether short or long trajectory contributes more significantly in the HHG process. We use the Gabor transform, which is a Fourier transform with a sliding Gaussian window [18]. The result is shown in Fig. 3. It is clear that one peak mainly contributes to the harmonics and the left channel is much more dominant than the right one, namely, the intensity of the recombination which corresponds to the long quantum path is several orders of magnitude less than that of the short quantum path. Since these two quantum paths have different emission times and phases, when several orders of the harmonic are superimposed, the irregular attosecond pulse trains will be obtained, and the electrons with long paths travel

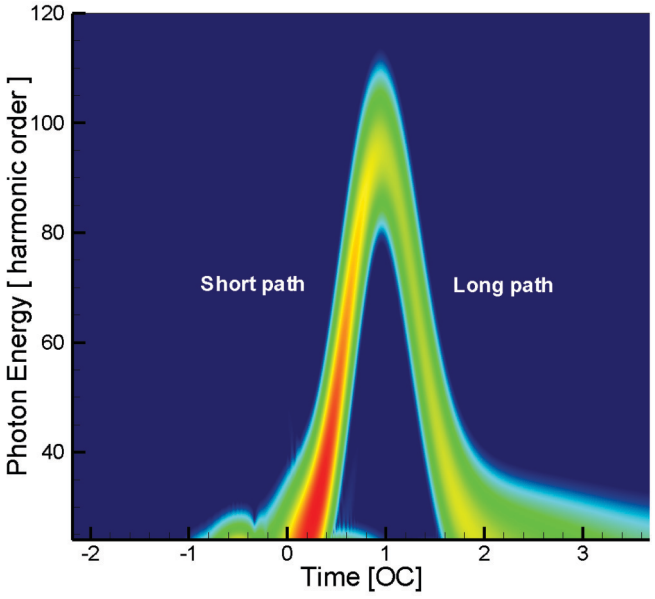

FIG. 3. (Color online) The quantum wavelet transform of the induced dipole acceleration as a function of the photon burst time and the photon energy performed by the Gabor transform for a two-color synthesized field containing half-cycle 800-nm driving and half-cycle 2000-nm control pulses.

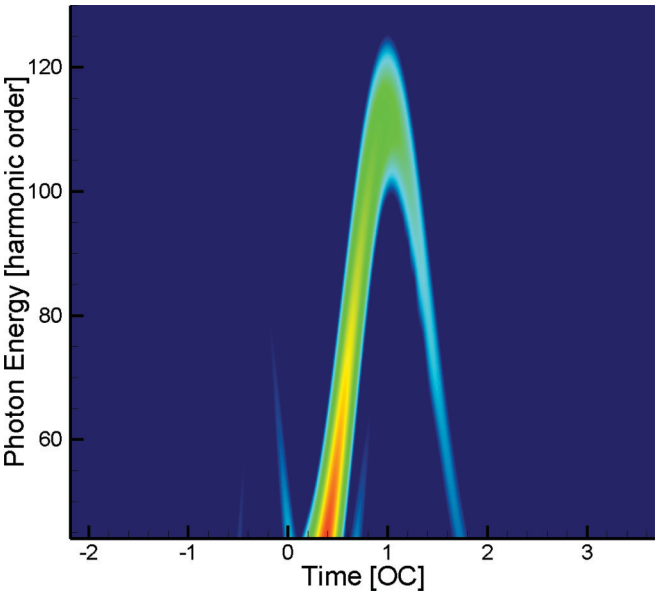

FIG. 4. (Color online) The quantum wavelet transform of the induced dipole acceleration as a function of the photon burst time and the photon energy for the two-color field synthesized by half-cycle 800-nm driving and half-cycle 2300-nm control pulses.

a longer time in continuous state than the short path, resulting in lower harmonic conversion due to the quantum diffusion. Nevertheless, the problems can be solved by filtering out a single quantum path. To do this, in our second attempt, we try to completely eliminate one path.

In our second attempt, the two-color laser pulses are synthesized via a half-cycle 800-nm driving pulse and a half-cycle 2300-nm pulse. Other parameters are the same as Fig. 1(a). With such scheme, the contribution of the control pulse in the ionization process is reduced, but it mainly affects the recombination step and extends the cutoff more than the first case. Many more electrons ionized by the leading half-cycle wave with higher intensity are driven back to its parent ion in the trailing longer half-cycle and release gained energy as emitted high energy photons. The quantum wavelet transform of $a(t)$ is shown in Fig. 4 which is obtained by a prolonged trailing pulse via a 2300-nm control pulse; whereas the short quantum path dominantly contributes in the HHG process, the long path has not been completely eliminated. Figure 5 shows the HHG spectrum of this waveform. It can be seen that the cutoff has been extended more than that of a half-cycle 2000-nm pulse shown in Fig. 2. On the other hand, whereas the modulation between harmonics has been extremely reduced in the middle of the plateau, they appear in the end of plateau, so it can be deduced that the contributions of both quantum paths are comparable in the near-cutoff region.

In the next step, to completely eliminate the long path, we prolong the leading of waveform via a half-cycle 2600-nm pulse. The resulting HHG spectrum is shown in Fig. 5. It can be seen that despite some minor fluctuation, as shown by a dash-dotted black ellipse, the harmonics spectra is approximately uniform in all areas of the spectrum. Therefore, in comparison with $\lambda_c = 2300$ nm, we expect the long path should be completely eliminated. Before the investigation of

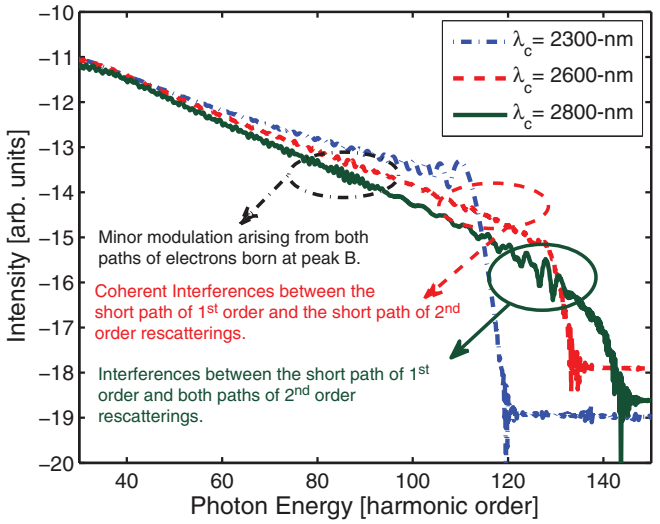

FIG. 5. (Color online) The harmonic spectrum of a helium atom exposed to the two-color field synthesized by half-cycle 800-nm driving and the prolonged control fields described in the the figure key.

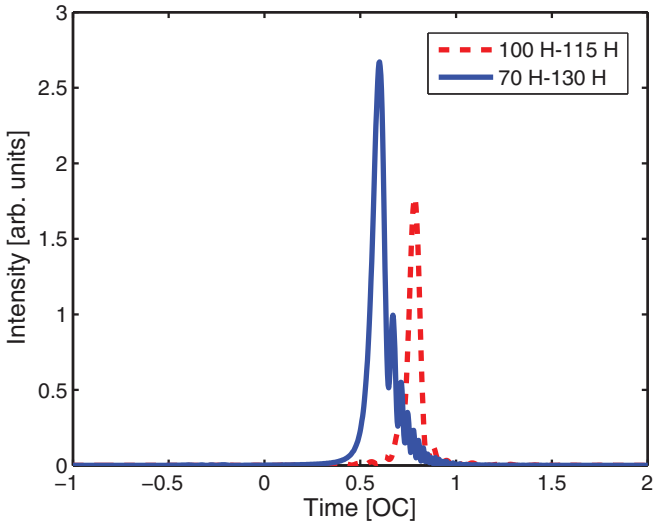

FIG. 6. (Color online) Isolated attosecond pulse (solid line) calculated by synthesizing the all continuum and isolated attosecond pulse (dashed line) calculated by synthesizing the 100th–115th harmonics obtained from the harmonics spectra of Fig. 5 for $\lambda_c = 2600$ nm.

electron dynamics contributed in this modulation, to show that the presented waveform supports the isolated attosecond pulse generation, we will consider the attosecond pulse generation from the HHG spectrum. In spite of minor modulation, it can be expected that this spectrum can support the generation of a clear single attosecond pulse. By selecting a frequency window to the supercontinuum spectrum and making an inverse Fourier transformation, an attosecond pulse is generated. Now let us discuss the selected frequency window. With a given frequency window, if we move this window along the harmonic order axis, the duration of the attosecond pulse changes a little, though the intensity decreases. That is to say, the pulse duration is not sensitive to the position of the frequency window. One may think that if we enlarge the width of the frequency window, the attosecond pulse duration will shorten further. Actually, due to the phase mismatch, the pulse lengthens rather than becoming shorter. It has been suggested that the bandwidth of the attosecond pulse is more important than the duration in attosecond science [29]; hence, we take into account the whole supercontinuum in the attosecond pulse generation. Through synthesizing 70th–130th harmonics in the second case $\lambda_c = 2600$ nm, the attosecond temporal profile is shown by a solid line in Fig. 6. Whereas the selected frequency window is broader, only a 185 as isolated attosecond pulse is emitted. Our results show that without any phase compensation, the intensity of the attosecond pulse for the combined sub-one-cycle pulses is several times stronger than that for the single-color laser. If the phase dispersion is properly compensated, a sub-50 as pulse will be generated. All of these advantages arise from the elimination of the long quantum path in the HHG process. In spite of some fluctuations around the main peak—whereas the selected frequency window is broader—due to good phase matching conditions, an isolated attosecond pulse is directly obtained. Through synthesizing the 100th–115th harmonics in the second case $\lambda_c = 2600$ nm, the attosecond temporal profile is shown by a dashed line in Fig. 6. With selected frequency window, a 170-as isolated pulse is emitted. In comparison to the neighbor pulse, the signal-to-noise ratio of this pulse is higher so this pulse has rather fine appearance. In both cases, not only the short paths of first-order rescattering contribute in the structure of harmonics supporting such attosecond pulses, but also the short path of second returned electrons contribute in their structure. To examine whether such a claim is correct or not, we should consider the time-energy analysis of the photon energy at the photon burst time.

To find the quantum paths that contributed to some minor modulations appearing in the HHG spectrum of the second case $\lambda_c = 2600$ nm, we plot the quantum wavelet transform of $a(t)$ in Fig. 7(a). This figure, in comparison with the corresponding wavelet transform $a(t)$ for $\lambda_c = 2300$ nm shown in Fig. 4, has two distinct differences. First, a subpeak appears to the left of the main peak. Second, while the long path of the main peak is completely suppressed, more quantum paths appear below the main peak. The first one arises mainly from electrons born at peak B shown in Fig. 1(a). When the control wavelength increases up to 2600 nm, the control pulse cannot effectively contribute in the ionization process, because peak C drops down and the ionization rate reduces. Therefore, unlike the first attempt, the quantum paths related to electrons born at B, because of their considerable intensity, create some minor modulation in the HHG spectra where the harmonics order is lower than 90 as shown by a dash-dotted black ellipse in the Fig. 5.

To find the electron dynamics of the quantum paths appearing below the main peak, we examine a more prolonged trailing. In the final attempt, we prolong the trailing of the waveform via a half-cycle 2800-nm pulse. The HHG spectrum of this waveform has been shown in Fig. 5. In comparison to $\lambda_c = 2600$ nm, a half-cycle 2800-nm pulse extends the cutoff more but some considerable modulation appears in the end

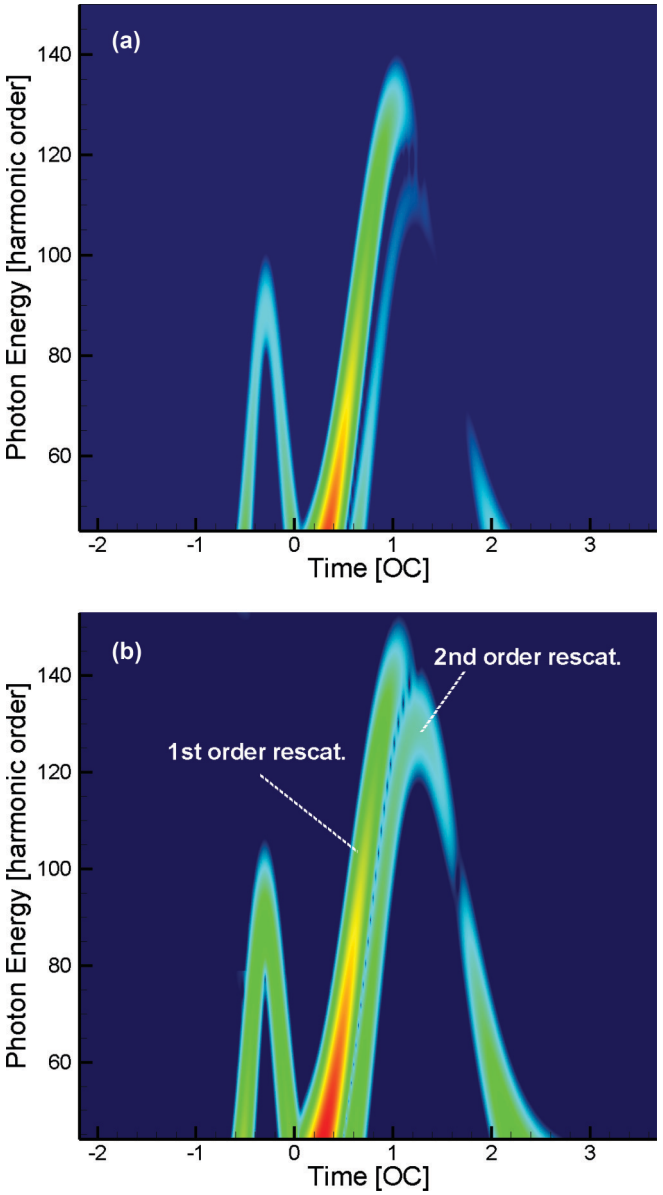

FIG. 7. (Color online) The quantum wavelet transform of the induced dipole acceleration as a function of the photon burst time and the photon energy for the two-color field synthesized by the half-cycle 800-nm driving pulse and the (a) half-cycle 2600-nm control pulse and (b) half-cycle 2800-nm control pulse.

section of the spectrum shown by a solid green ellipse in Fig. 5. The physics underlying this waveform can be explained with the aid of the time-frequency analysis shown in Fig. 7(b). This plot shows the HHG emission time for electrons at the moment of rescattering. According to this figure, HHG emission arises from the first and second consecutive rescatterings of the different electron trajectories with the parent ion. It can be seen that the contribution of short paths in the second rescattering is more than that of the long path. In the optimized conditions such as the 2600-nm case, the appearance of a fine structure in the x-ray pulses can be connected to the increase in relative strength of the HHG emission from the second rescatterings of the electron wave packet with the ion, as the control laser wavelength is increased. The interference structures become significant if the relative weights of HHG emission from the first and subsequent rescatterings are comparable. This occurs on the trailing edge of the laser pulse, where the efficiency loss associated with electron wave-packet spreading for the second rescatterings is compensated by the higher ionization rate when the electron was liberated into the continuum. In the 2800-nm case, it can be concluded that the considerable modulation in the end section of the HHG spectrum shown by a solid green ellipse in Fig. 5, originates mostly from interferences between short and long paths of the second-order rescattered electrons. The most interesting feature is the fine structure of harmonics spectrum at high photon energies which happens in the prolonged trailing with $\lambda_c = 2600$ nm. The short paths of the first and second consecutive rescatterings of the different electron trajectories shown in Fig. 7(a) contribute in the structure of harmonics shown by a dashed red ellipse in Fig. 5. These structures are not observed using near-IR driving laser wavelengths around 800 nm, and are only present when mid-IR driving fields are used. In our simulations, they appear gradually during the interaction, and mainly influence the x-ray bursts generated on the trailing part of the mid-IR pulse. Note that the relevance of higher-order rescatterings for strong-field processes at multicycle longer wavelengths has been recently described in other contexts as well, theoretically [26] and experimentally [30], although its technological potential was not identified. As a final result, it can be noted that the effect of the prolonged trailing scheme can be considered from a macroscopic level, namely, through prolonging the trailing of a two-color waveform, the contribution of the control pulse in the ionization process is reduced, but it mainly affects the recombination step. The effects of such scheme can be considered from a macroscopic and a microscopic view. In the microscopic level, the short path of consecutive rescatterings can coherently contribute in the harmonics spectra, which leads to enhancement of the harmonic yields. In the macroscopic level, the reduction of the ionization rate leads to the reduction of the ionization-induced mismatching of the harmonics in the ionized media. It is clear that high-order quantum paths recontribute in the harmonic spectra and compensate the reduction of ionization rate effects on the converted efficiency.

IV. CONCLUSION

In conclusion, we present an efficient scheme to contribute the consecutive electron rescatterings in the extreme ultraviolet supercontinuum based on synthesized two-color pulses. Subcycle near-IR and mid-IR pulses construct the leading and the trailing of waveform, respectively, thereby tunnel ionization and recombination as the first and third step in the well-known three-step model are manipulated. It means that the pulses are offset in time so that at early times the near-IR mostly dominates and at later times the mid-IR dominates. We show such scheme can generate a broad supercontinuum which supports isolated attosecond pulses. Quantum wavelet analysis shows under prolonged trailing, in addition to suppressing of the long path for first returned electrons, quantum paths of higher-order rescatterings appear and contribute in the spectrum. These quantum paths can create some unwanted modulations in the spectrum because of interferences between the short and the long paths of

high-order rescatterings. With an efficient scheme, the short paths of the first and second consecutive rescatterings of the different electron trajectories contribute in the structure of high harmonics that leads to a fine appearance in the x-ray pulses. Hence, the contribution of consecutive rescatterings has at least two main aspects. First, it enhances the harmonics yields. Second, at the macroscopic level, owing to a decreased ionization rate, and therefore a reduction of propagation phase mismatching effects, the generated attosecond pulse will have fine appearance. Interestingly, the contribution of consecutive rescatterings in harmonics spectra compensates the effects of reduction of accessible ionized atoms on the converted harmonics efficiency. The low converted efficiency and the weak pulse appearance are two crucial defects in the attosecond pulse generation and are still an open problem. Then based on the model results, the crucial defects can be decreased through the contribution of consecutive rescatterings in the HHG process.

[1] P. B. Corkum and F. Krausz, Nat. Phys. **3**, 381 (2007).

[2] M. Drescher, M. Hentschel, R. Kienberger, M. Uiberacker, V. Yakovlev, A. Scrinzi, Th. Westerwalbesloh, U. Kleineberg, U. Heinzmann, and F. Krausz, Nature (London) **419**, 803 (2002).

[3] M. Uiberacker, Th. Uphues, M. Schultze, A. J. Verhoef, V. Yakovlev, M. F. Kling, J. Rauschenberger, N. M. Kabachnik, H. Schröder, M. Lezius, K. L. Kompa, H.-G. Muller, M. J. J. Vrakking, S. Hendel, U. Kleineberg, U. Heinzmann, M. Drescher, and F. Krausz, Nature (London) **446**, 627 (2007).

[4] T. Brabec and F. Krausz, Rev. Mod. Phys. **72**, 545 (2000).

[5] G. Sansone, E. Benedetti, F. Calegari, C. Vozzi, L. Avaldi, R. Flammini, L. Poletto, P. Villoresi, C. Altucci, R. Velotta, S. Stagira, S. De Silvestri, and M. Nisoli, Science **314**, 443 (2006).

[6] D. B. Milosevic, J. Phys. B: At., Mol., Opt. Phys. **33**, 2479 (2000).

[7] D. Oron, Y. Silberberg, N. Dudovich, and D. M. Villeneuve, Phys. Rev. A **72**, 063816 (2005).

[8] Z. Chang, Phys. Rev. A **76**, 051403(R) (2007).

[9] K. Zhao, Q. Zhang, Michael Chini, Y. Wu, X. Wang, and Z. Chang, Opt. Lett. **37**, 3891 (2012).

[10] J. L. Krause, K. J. Schafer, and K. C. Kulander, Phys. Rev. Lett. **68**, 3535 (1992).

[11] K. J. Schafer, Baorui Yang, L. F. DiMauro, and K. C. Kulander, Phys. Rev. Lett. **70**, 1599 (1993).

[12] X. H. Song, Z. N. Zeng, Y. X. Fu, B. Cai, R. X. Li, Y. Cheng, and Z. Z. Xu, Phys. Rev. A **76**, 043830 (2007).

[13] R. López-Martens, K. Varjú, P. Johnsson, J. Mauritsson, Y. Mairesse, P. Salières, M. B. Gaarde, K. J. Schafer, A. Persson, S. Svanberg, C. G. Wahlström, and A. L'Huillier, Phys. Rev. Lett. **94**, 033001 (2005).

[14] C. Altucci, V. Tosa, and R. Velotta, Phys. Rev. A **75**, 061401(R) (2007).

[15] J. G. Chen, S. L. Zeng, and Y. J. Yang, Phys. Rev. A **82**, 043401 (2010).

[16] Z. Zeng, Y. Leng, R. Li, and Z. Xu, J. Phys. B: At., Mol., Opt. Phys. **41**, 215601 (2008).

[17] B. Zeng, Y. Yu, Wei Chu, J. Yao, Y. Fu, H. Xiong, H. Xu, Y. Cheng, and Z. Xu, J. Phys. B: At., Mol., Opt. Phys. **42**, 145604 (2009).

[18] M. Dashcasan, Opt. Commun. **318**, 216 (2014).

[19] S.-F. Zhao, X.-X. Zhou, P.-C. Li, and Z. Chen, Phys. Rev. A **78**, 063404 (2008).

[20] J. Xu, B. Zeng, and Y. Yu, Phys. Rev. A **82**, 053822 (2010).

[21] I.-L. Liu, P.-C. Li, and S.-I. Chu, Phys. Rev. A **84**, 033414 (2011).

[22] C. L. Xia and X. S. Liu, Phys. Rev. A **87**, 043406 (2013).

[23] P. Lan, E. J. Takahashi, and K. Midorikawa, Phys. Rev. A **81**, 061802(R) (2010).

[24] F. Calegari, C. Vozzi, M. Negro, G. Sansone, F. Frassetto, L. Poletto, P. Villoresi, M. Nisoli, S. De Silvestri, and S. Stagira, Opt. Lett. **34**, 3125 (2009).

[25] L. E. Chipperfield, J. S. Robinson, J. W. G. Tisch, and J. P. Marangos, Phys. Rev. Lett. **102**, 063003 (2009).

[26] J. Tate, T. Auguste, H. G. Muller, P. Salières, P. Agostini, and L. F. Di Mauro, Phys. Rev. Lett. **98**, 013901 (2007).

[27] G. Doumy, J. Wheeler, C. Roedig, R. Chirla, P. Agostini, and L. F. DiMauro, Phys. Rev. Lett. **102**, 093002 (2009).

[28] P. Antoine, B. Piraux, and A. Maquet, Phys. Rev. A **51**, R1750 (1995).

[29] G. L. Yudin, A. D. Bandrauk, and P. B. Corkum, Phys. Rev. Lett. **96**, 063002 (2006).

[30] D. D. Hickstein, P. Ranitovic, S. Witte, X.-M. Tong, Y. Huismans, P. Arpin, X. Zhou, K. E. Keister, C. W. Hogle, B. Zhang, C. Ding, P. Johnsson, N. Toshima, M. J. J. Vrakking, M. M. Murnane, and H. C. Kapteyn, Phys. Rev. Lett. **109**, 073004 (2012).